◆ Human Brain Mapping 6:250–269(1998) ◆

Influence of Skull Anisotropy for the Forward and Inverse Problem in EEG: Simulation Studies Using FEM on Realistic Head Models

Gildas Marin,[1] Christophe Guerin,[2] Sylvain Baillet,[1] Line Garnero,[1]* and Gérard Meunier[3]

[1]*Cognitive Neurosciences and Cerebral Imaging, Hôpital la Salpêtrière, CNRS UPR 640, Université Paris VI, 75651Paris Cedex 13, France, and Institut d'Optique Théorique et Appliquée, CNRS URA 14-Université Paris XI, Faculté d'Orsay. Orsay 91403, France*
[2]*Cedrat Recherche, Meylan 38246, France*
[3]*Laboratoire d'Electrotechnique de Grenoble, CNRS UMR 5529 INPG/UJF, 38402 St. Martin d'Hères, France*

Abstract: For the sake of realism in the description of conduction from primary neural currents to scalp potentials, we investigated the influence of skull anisotropy on the forward and inverse problems in brain functional imaging with EEG. At present, all methods available for cortical imaging assume a spherical geometry, or when using realistic head shapes do not consider the anisotropy of head tissues. However, to our knowledge, no study relates the implication of this simplifying hypothesis on the spatial resolution of EEG for source imaging.

In this paper, a method using finite elements in a realistic head geometry is implemented and validated. The influence of erroneous conductivity values for the head tissues is presented, and results show that the conductivities of the brain and the skull in the radial orientation are the most critical ones.

In the inverse problem, this influence has been evaluated with simulations using a distributed source model with a comparison of two regularization techniques, with the isotropic model working on data sets produced by a nonisotropic model. Regularization with minimum norm priors produces source images with spurious activity, meaning that the errors in the head model totally annihilate any localization ability. But nonlinear regularization allows the accurate recovery of simultaneous spots of activity, while the restoration of very close active regions is profoundly disabled by errors in the head model.

We conclude that for robust cortical source imaging with EEG, a realistic head model taking anisotropy of tissues into account should be used. *Hum. Brain Mapping 6:250–269, 1998.*

Key words: EEG; FEM; forward problem; inverse problem; anisotropic conductivity

INTRODUCTION

Among the rapidly advancing functional modalities of cerebral imaging, electroencephalography (EEG) together with magnetoencephalography (MEG) are the only ones which offer millisecond responses to brain activity. Actually, the imaging ability of these techniques is limited by the difficulty of the inverse problem,

Contract grant sponsor: MENRT; Contract grant number: Life Sciences Grant ACC-SV12.

*Correspondence to: Line Garnero, Neurosciences Cognitives et Imagerie Cérébrale, LENA-CNRS UPR-640, Hôpital de la Salpêtrière, 47 bd. de l'Hôpital, 75651 Paris Cedex 13, France. Fax: 33(0)1 44 24 39 54; E-mail: lenalg@ext.jussieu.fr

Received for publication 18 June 1997; accepted 6 April 1998

which has to provide the localizations of the neural sources inducing the measurements. This inverse problem is ill-posed in EEG or MEG due to the nonunicity of the solution and the weak number of recorded data compared to the data available in PET or f-MRI.

For these reasons, the first proposed and still the most commonly used approach to the inverse problem consists in fitting one or a few equivalent current dipolar sources (ECD) to the potential map by nonlinear estimation techniques [Sherg and Buchner, 1993]. Although this model can well describe the focal activities induced by a simple somatosensory study, it is inadequate to represent complex neural networks or distributed activities along cortical surfaces. In order to overcome these difficulties, different tomographic reconstruction techniques have been proposed which estimate a distribution of current vectors on a regular surface grid [Hämäläinen and Ilmoniemi, 1984] or a volume grid [Pascual-Marqui et al., 1994] or cortical surface deduced from MRI images [Dale and Sereno, 1993]. The ''distributed sources'' inverse problem consists in solving a set of linear equations, since the locations of the currents are imposed, but this system is undetermined since there are many more unknowns than the number of data. Then constraints must be introduced in order to limit the set of admissible solutions in a so-called regularization scheme. The most commonly used are minimum norm estimates (Hämäläinen and Ilmoniemi, 1994; Wang et al., 1992] or quadratic regularizations that generate smooth distributions, not corresponding to realistic physiological solutions. Some extensions of quadratic procedures can sharpen these diffuse solutions during iterative processing of quadratic inversion [Gorodnitsky et al., 1995]. We developed a nonlinear regularization technique S-MAP, the main originality of which is to use functional and anatomical information not only to constrain the positions and orientations of the currents but also to directly guide the regularization process along the cortical surface [Baillet and Garnero, 1997]. This method prevents smoothing of dipole amplitudes between two adjacent cortical zones with functionally decorrelated activities (as may happen between two walls of a sulcus, or a sulcus and its adjacent gyrus). It can then provide a physiologically plausible description of the neural sources.

The distributed source inverse problem is also very ill-posed. The solutions are very sensitive to noise, and most of the regularization methods consider this problem. Inverse solutions also depend on the mathematical model which links the source amplitudes to the electrode potentials (the so-called forward problem), where local conductivities play an essential role. Little is known on this subject. For this reason we address here the question of the influence of head modelling approximations, such as the assumption of skull isotropic conductivity, on the solutions of the EEG inverse problem.

Different head models have been used, and the complexity of the corresponding potential calculations increases with the accuracy of the head description. The simplest and the most commonly used is the three or four concentric sphere model with homogeneous conductivity values which represent the skin, the skull, the Cerebrospinal Fluid (CSF), and the brain tissues. In this case, analytical expressions have been derived to calculate the scalp potentials [De Munck, 1988]. Spherical models may take into account anisotropy of the medium by assigning constant radial and tangential conductivities to the skull shell, but they give a poor approximation of head shape. In order to take into account realistic head geometry, Hämäläinen and Sarvas [1989] used the boundary element method (BEM), which is adequate for piecewise homogeneous isotropic media. However, BEM cannot be applied when some inhomogeneities are present (such as skull holes) or when the medium has an anisotropic conductivity. Indeed, anisotropy influences the scalp potential distributions [Peters and de Munck, 1990]. In such a case, the finite element method (FEM) allows one to consider accurate inhomogeneous realistic models, since it computes the Maxwell equations very locally. Different authors have developed FEM methods [Yan et al., 1991; Bertrand et al., 1991; Haueisen et al., 1995; Buchner et al., 1997; Awada et al., 1997]. FEM is difficult to implement since it requires volume meshes of the different head tissues, which are more complex to derive than the surface meshes used by BEM. For this reason, FEM is less commonly used than BEM, even though it is more accurate.

Considering this fact, the relevant questions are: *is it absolutely necessary to use FEM in order to accurately compute the solution of the EEG inverse problem? Furthermore, under what conditions can BEM provide accurate solutions?* The most pertinent way to answer these questions is to evaluate the role of anisotropies in the electrical conductivities of brain tissues [Wikswo et al., 1993] and particularly the bone anisotropy, since the presence of the skull greatly influences the scalp potential distribution. Such influence has been evaluated in the forward and inverse dipolar problem by Peters and de Munck [1990] with analytical methods, and by Thevenet [1992] with FEM in a spherical head model. FEM has also been used with a realistic head model [Haueisen et al., 1997], but those authors only

studied the influence of conductivity values on the scalp distribution.

In this work, the influence of skull anisotropy is evaluated for the forward and inverse problem, in both a spherical and in a realistic head model. We computed these two models in order to check whether or not the influence of conductivities depends on head geometry. For the inverse problem we considered the distributed source model only, because it is certainly the most powerful way to describe brain electrical activity and because the distributed inverse solution is more disturbed by forward model errors than the dipolar one. To our knowledge, no such study has yet been published. As we have seen, the solution also greatly depends on the regularization method, which constrains the source space. For this reason we considered different regularization schemes: a quadratic regularization and the S-MAP method.

More precisely, for this study, FEM is implemented and validated in the spherical case in comparison with analytical results, and the optimum characteristics of the numerical methods are derived. Then the influence of skull anisotropy on scalp potential is evaluated by comparing the distributions obtained with and without anisotropy both in a spherical and in a realistic head model. To derive the influence of the skull isotropic conductivity approximation in the inverse problem, the gain matrix is computed with an isotropic forward model and a distributed source model is reconstructed with this matrix from data simulated with FEM and an anisotropic skull model. As for the forward problem, spherical and realistic head models are considered and the reconstructions are computed with the different regularization methods mentioned above. *We have checked that each inverse method succeeds at recovering accurately the source distribution when the gain matrix is computed with the right anisotropic model.*

The method is presented in the first section: we review the formulation of the forward problem and briefly present FEM (the formulation is described in the Appendix). The construction of our head model is then detailed. In the second section, FEM is validated and a study of the influence of element size and element order is presented. The influence of anisotropy is discussed in the following sections with regard to the forward problem and the inverse problem.

METHODS

Finite element method

In the EEG forward problem, the computation of the scalp potential, assuming a source current density, requires solving the Poisson equation in a given head model (see Appendix, Equation 3). The head is made of different media k which can be either isotropic or anisotropic, each medium being characterized by a conductivity tensor $[\sigma_k]$. This tensor reduces to a scalar value when the conductivity of the medium is isotropic.

When solving the Poisson equation, a singularity appears at the dipole position which may cause numerical problems. An elegant way to avoid this singularity is to split the potential V in two parts: where V_s, called the ''singular solution,'' is the potential due to the dipole in an infinite homogeneous medium that has the same conductivity as that of the medium containing the dipoles. U, called the ''regular solution'' or ''reduced potential,'' remains finite at each point [Bertrand et al., 1991; Awada et al., 1997]. Awada et al. [1997] have shown, in the two-dimensional (2D) case, that this so-called ''substraction method'' leads to better accuracy than direct computation of V when the current source is explicitly implemented in the model [Haueisen et al., 1995; Buchner et al., 1997]. The originality of our method, as detailed in the Appendix, is the possibility for computing either the reduced potential or the total potential in media that do not contain sources; we show that computing the total potential in the scalp rather than the reduced potential improves the accuracy of the method (see Influence of Anisotropy on the Forward Problem, below). Furthermore, the FEM formalism has been extended in order to modelize anisotropic conductivities (see Appendix, Equation 8).

In practice, we have implemented the forward problem on the software Flux3d developed by the Laboratoire d'Electrotechnique de Grenoble (St. Martin d'Hères, France), and commercialized by the Cedrat Recherche Company (Meylan, France).

Model construction

Model geometry and mesh generation

All the models we use contain three separate media: the scalp, the skull, and the brain. In this study, the skull is assumed to be the only part that may have anisotropic conductivity. Meshes of three concentric spheres have been generated for comparison with the analytical method. The radii of different media are taken to be 10 cm for the scalp, 9.2 cm for the skull, and 8.7 cm for the brain. The realistic geometry-based mesh has been generated from 56 segmented MRI pictures of the head [Zubal et al., 1994] with 256 $\times$ 256 pixels. These are manually segmented images, where the different media can be separated with a single thresholding. The head is split in three concentric media and

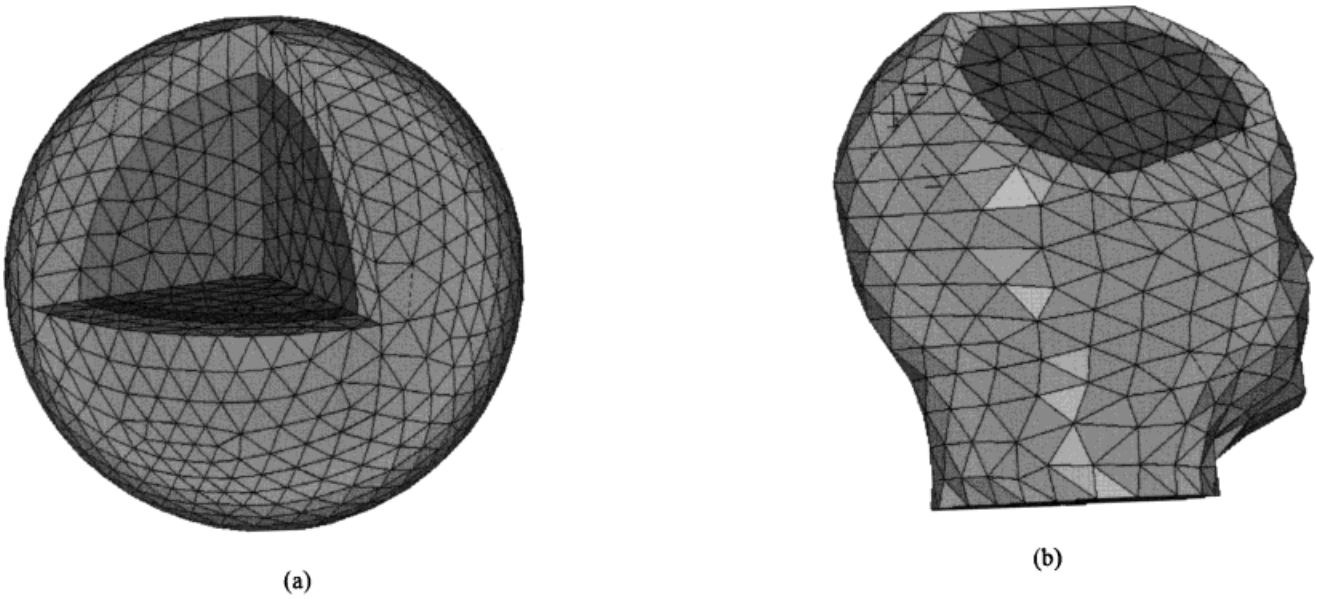

Figure 1.
Inside view of the tetrahedric mesh of **(a)** the three-shells spherical model, and **(b)** the realistic head model.

a three-dimensional morphologic smoothing is made on each shape, so that they may be meshed more easily. Some more complicated anatomical parts such as ears and upper and lower jaw bones have been removed. A bidirectional mesh of spline curves is obtained, starting with regularly spaced contour points of MRI (20 points per image). A spline surface, derived from these curves, accurately models the surface between two consecutive media. Each spline surface is tesselated with triangular elements, and the tetrahedric mesh of each medium is derived from these boundary surface meshes. Since the internal surface mesh of the scalp (respectively, the skull) is the same as the external mesh of the skull (respectively, the brain volume), the volume meshes of the three shells are perfectly interconnected. This is illustrated in Figure 1a with an internal view of the spherical mesh, and in Figure 1b with a view of the realistic mesh obtained by cutting the head volume with an oblique plane. These surface meshes are also used to define the tensor direction of the anisotropic elements (see Model Conductivity, below).

Two types of elements are considered: linear tetrahedrons (first-order elements) and parabolic tetrahedrons (second-order elements). Linear tetrahedrons are classical tetrahedrons with four nodes and plane surfaces. Parabolic tetrahedrons have 10 nodes (one more at the middle of each edge) and parabolic surfaces. With the first type, the basis functions w_i, defined in the Appendix, are linear functions, whereas with the second type, these are parabolic functions; the approximation of the potential is more precise in the second case (see FEM Validation, below). Spherical meshes have been generated with five different element sizes in order to study the influence of mesh size on the solution. Table I presents the characteristics of the different meshes that have been used. Figure 2 shows the realistic head mesh and two of the spherical meshes. We do not use locally refined meshes. Indeed, although the forward problem has been validated with one dipole only, the inverse problem has been solved with a distributed source model (see Influence of Anisotropy on the Forward Problem, below). Local

TABLE I. Characteristics of elements of volume meshes

Name	Element size	Number of elements	Number of nodes	Element order
sph20_1	20 mm	8,329	1,307	1
sph20_2	20 mm	8,329	9,486	2
sph15_1	15 mm	15,141	2,366	1
sph15_2	15 mm	15,141	17,454	2
sph12_1	12 mm	26,359	4,129	1
sph12_2	12 mm	26,359	30,452	2
sph10_1	10 mm	41,368	6,527	1
sph10_2	10 mm	41,368	62,502	2
sph8_1	8 mm	73,422	11,647	1
sph8_2	8 mm	73,422	87,907	2
head10_1	10 mm	43,742	8,400	1
head10_2	10 mm	43,742	62,563	2

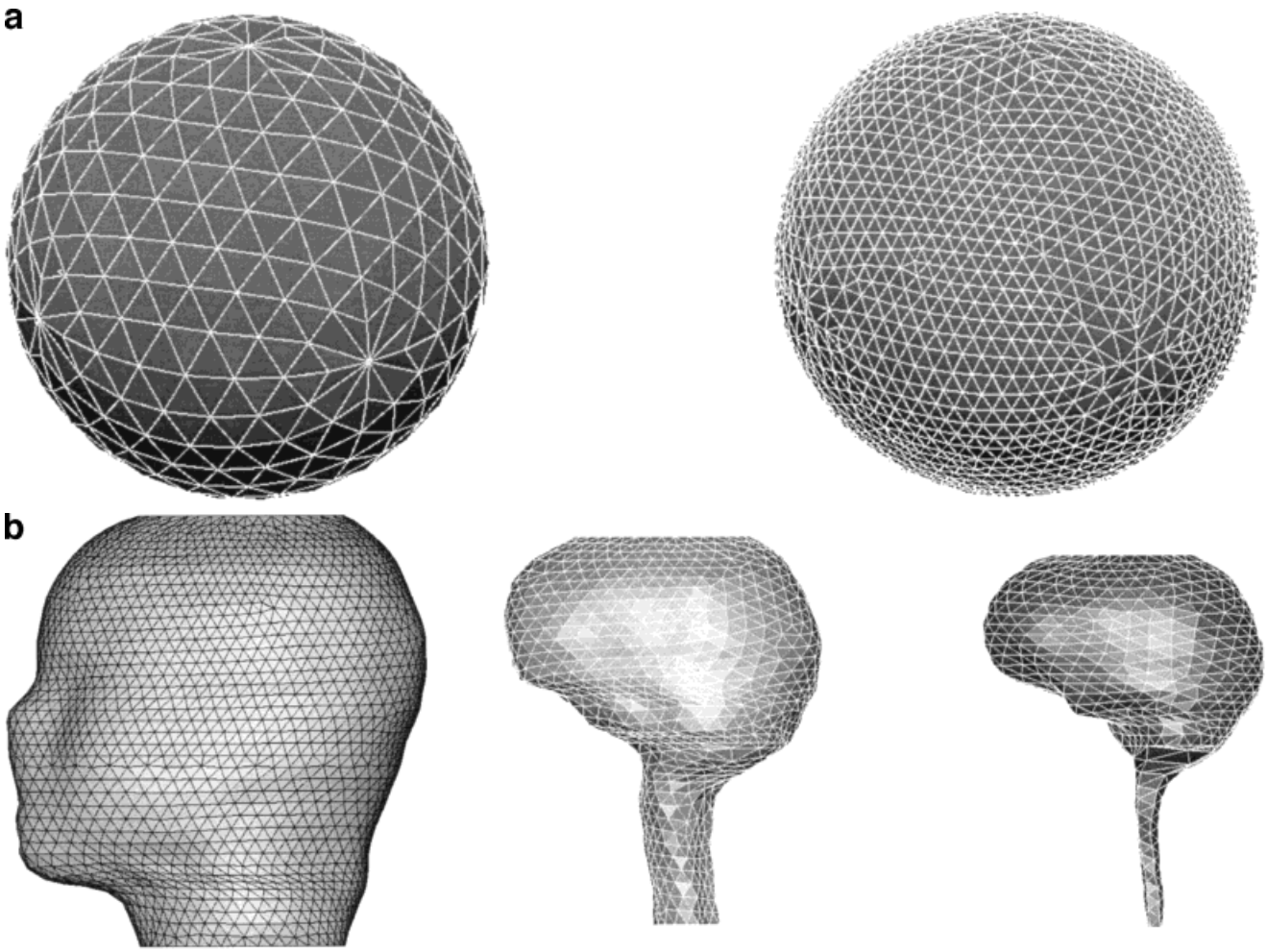

Figure 2.
Meshes used for FEM. **a:** Spherical mesh with the largest element size (8,329 elements) and the smallest element size (73,422 elements). **b:** Realistic head mesh (total, 43,742 elements), with skin (27,543 elements), skull (6,110 elements), and brain (10,089 elements).

refinement over every dipole location is then useless, since electrical activity may appear in many distinct regions of the cortex. We would thus rather use meshes with globally decreasing element size.

All meshes were generated on the software I-DEAS version VI.i (SDRC Company, USA).

Model conductivity

Table II gives the normalized conductivity values used for each medium. Radial and tangential directions are used to define the anisotropic conductivity tensor of the skull. In a the realistic model of the head, the radial direction in a volume element of the skull is defined as the normal to the triangular element of the external skull surface mesh that is the nearest to this volume element. The tangential directions are contained in the surface element plane (see Fig. 3).

FEM VALIDATION

FEM has been validated in the spherical case for different dipole locations by comparing the analytical potential distribution V_{real} with the FEM calculated distribution $V_{estimated}$. The dipole may be radial or

TABLE II. Normalized conductivities used for the models

Medium	Scalp	Skull	Brain
Tangential conductivity	1	0.125	1
Radial conductivity	1	0.0125	1

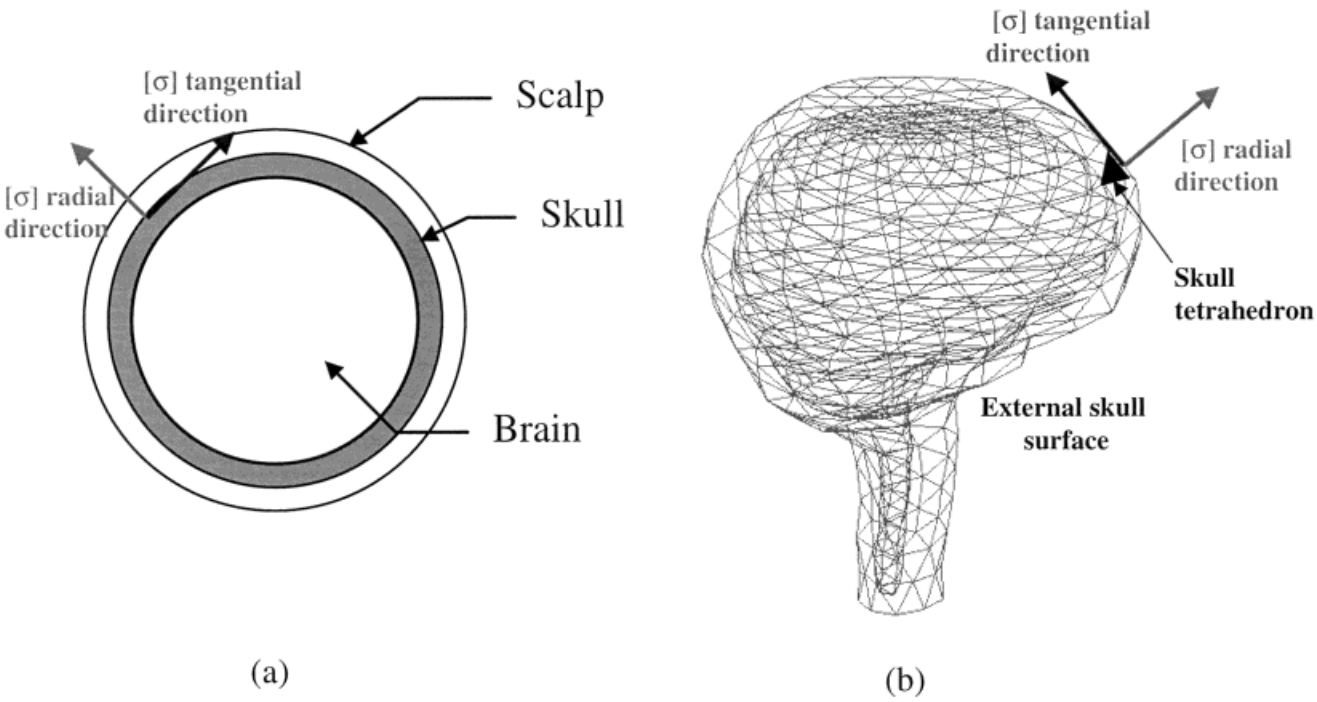

Figure 3.
Computation of the radial and tangential directions of the conductivity tensor at each element of the skull mesh. **a:** In a spherical model. **b:** In a realistic head model.

tangential and its position is defined by its eccentricity, which is the distance of the dipole from the sphere center divided by the radius of the external surface (eccentricity 1.0 corresponds to the external boundary of the scalp). The dipole eccentricity varies from 0.1–0.82. In all cases, the potential reference is chosen in such a way that the average potential on the external surface is zero. The analytical potential distribution V_{real} is calculated using the formula given in de Munck [1988].

Two error criteria introduced for BEM [Meijs et al., 1989], the ''relative difference measure'' (RDM) and the ''magnification factor'' (MAG), were computed. The RDM on a surface S is given by:

$$RDM_S = \left[\int_S \left(\frac{V_{real}}{\sqrt{\int_S V_{real}^2 dS}} - \frac{V_{estimated}}{\sqrt{\int_S V_{estimated}^2 dS}} \right)^2 ds \right]^{1/2};$$

the MAG is given by :

$$MAG_S = \left[\frac{\int_S V_{estimated}^2 ds}{\int_S V_{real}^2 ds} \right]^{1/2}.$$

The MAG gives an indication of errors in the magnitude of the potential, whereas the RDM indicates defects in the potential distribution on the surface.

Preliminary results were calculated for both isotropic and anisotropic models, using first-order (sph10_1) and second-order (sph10_2) meshes of 10-mm element size. Errors have been computed on the external boundary of the scalp for radial and tangential dipoles.

We will now consider two ways of improving the solution without increasing the number of elements. Since the skull conductivity is very small (by a factor of 80) compared to that of the other media, the potential collapses through it. The total potential V on the scalp is thus considerably lower than V_s and U. This means that the quantity $U + V_s$ in this medium is the difference of two numbers of approximately the same value and may thus have important numerical errors. The first way to improve the solution is to compute the total potential V in the scalp instead of the reduced potential U, though U remains the variable computed in the rest of the volume (i.e., the skull and brain). The continuity between adjacent media is given by Equation (5) of the Appendix. Of course, V still remains the interesting variable in all cases. In the regions where U is computed, the potential is given by the sum $U + V_s$, whereas in the scalp, V is directly given by the FEM

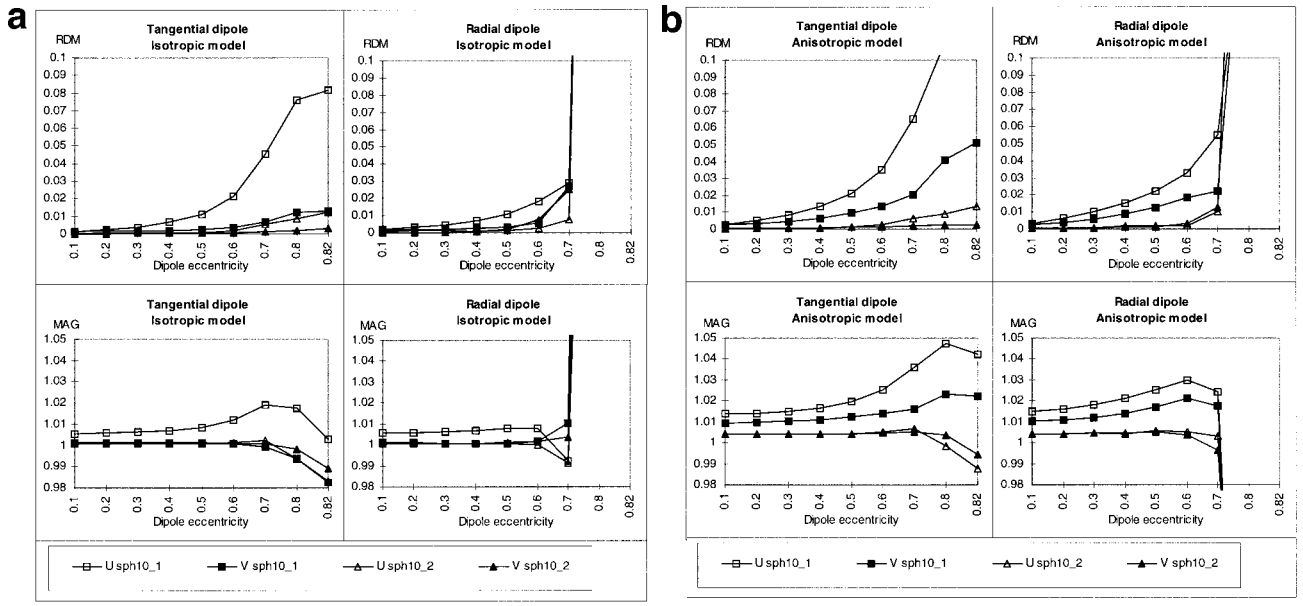

Figure 4.

Errors on the scalp potential distribution calculated with 10-mm element size meshes. Errors are shown for first-order elements (mesh sphere, 10-1) and second-order elements (mesh sphere, 10-2), and with either U or V computed in the scalp (whereas U is computed in the remaining volume). **a:** Isotropic model of the skull. **b:** Anisotropic model of the skull.

solution. The second way to further improve the solution is to use parabolic tetrahedrons. Replacing the first-order elements with second-order elements increases the computation times by 20–30% only.

Figure 4 shows the results with mesh sph10_1 and mesh sph10_2, when either *U* or *V* is computed in the scalp, assuming isotropic (Fig. 4a) or anisotropic skulls (Fig. 4b). Each part of Figure 4 shows the RDM and the MAG for the radial and the tangential dipoles. Computing the total potential *V* in the external medium instead of the reduced potential *U* significantly improves the solution. This is particularly true for eccentric tangential dipoles and when first-order elements are used. Figure 4 also shows that using second-order elements instead of first-order elements significantly improves the solution. In general, computing V in the scalp with second-order elements always improves the solution. In some cases, as for eccentric radial dipoles, the difference between the solutions obtained with U and V in the scalp is very small, since *V* is not low in this case. Figure 5a,b was obtained by computing *U* and *V*, respectively, in the scalp. It clearly appears that the distribution is smoother with the computation of *V*. Figure 6a,b shows the errors on the scalp for different element sizes using the optimal configuration (parabolic elements and computation of *V* in the scalp). Table III gives the times needed to compute a potential distribution on the scalp on an HP C110 workstation (Hewlett Packard). Both Figures 4 and 6 show that the errors in the anisotropic model are higher than those in the isotropic model for the first-order elements. However, they are practically the same with second-order elements. In the region of low eccentricities, the curves for the radial and the tangential dipoles (e.g., the RDM of Fig. 4a) are practically identical. However, in the domain of high eccentricities, the increase for the case of the radial dipole is extremely fast.

In conclusion, good accuracy is obtained for the tangential dipole with the mesh sph12_2, when the eccentricity does not exceed 0.8. For higher eccentricity, the mesh sph10_2 is necessary to have good accuracy. For the radial dipole, mesh sph10_2 allows great accuracy for eccentricities lower than 0.7. For eccentricities higher than 0.8, it was not possible to obtain accurate results even with our finest mesh of 8-mm elements. Mean values for normalized minimum and maximum radii defining the cortex volume are 0.64 and 0.84 [De Munck, 1989; Peters and de Munck, 1990]. Thus, most of the dipoles that are located in the cortex will have an eccentricity lower than 0.8. This means that 10-mm element size meshes will be sufficient in most cases, and even 12-mm element size meshes should be sufficient in the case of

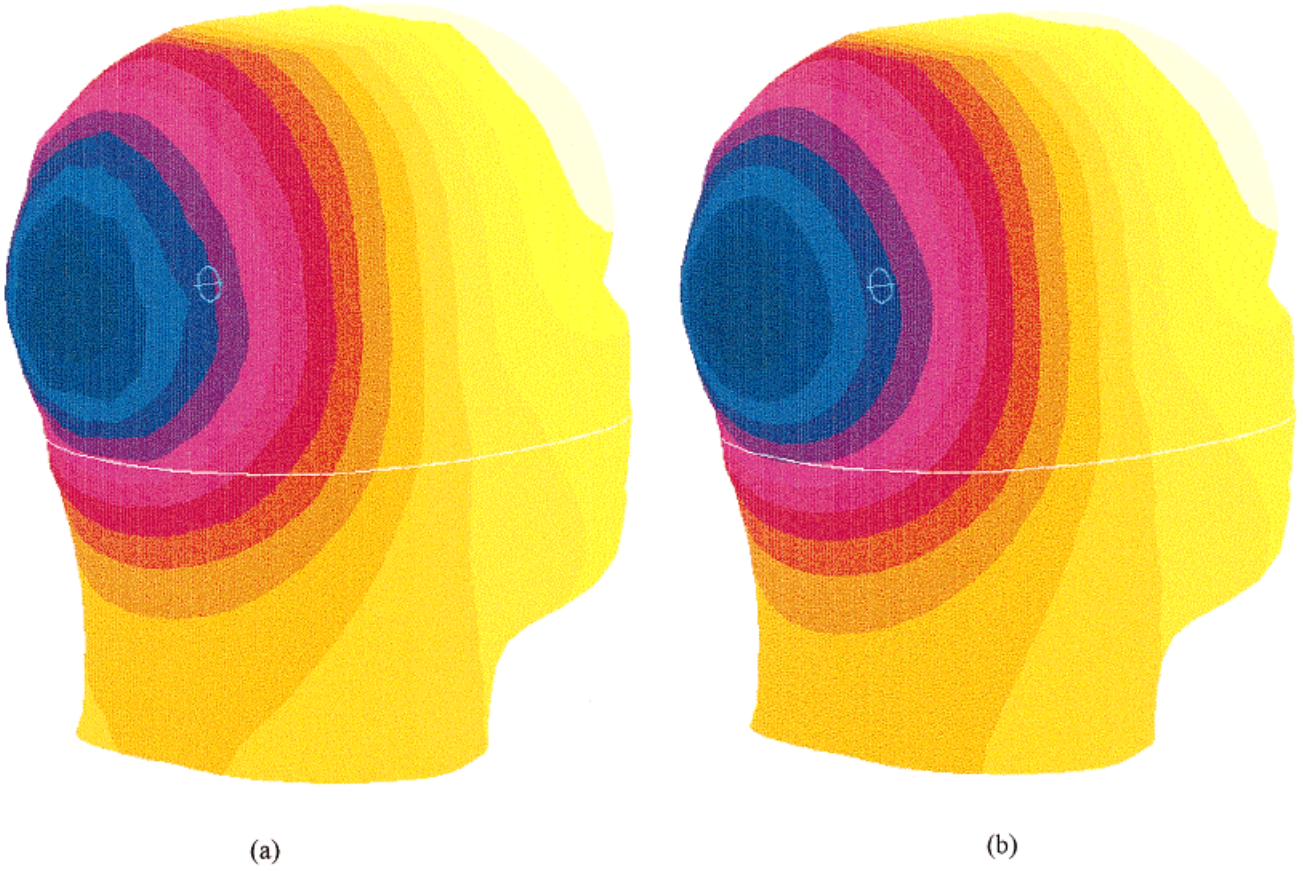

Figure 5.
Potential distribution calculated with **(a)** computation of U in the scalp and **(b)** computation of V in the scalp. Note that in the second case, the distribution is more regular because numerical errors are minimized.

tangential dipoles. But for radial dipoles, considering that FEM requires reasonable element size meshes, the eccentricity has to be limited to 0.7, which is a middle value for the cortex. These results are similar to those described elsewhere [Bertrand et al., 1991; Awada et al., 1997].

INFLUENCE OF ANISOTROPY ON THE FORWARD PROBLEM

In this section, the influence of the conductivity tensor on the potential distribution of the scalp is discussed.

Variation of the magnitude of conductivity

First, the influence of conductivity values is studied for each medium, using the analytical model in the spherical case. This study was made with a dipole of 0.6 eccentricity, which is a value that leads to an accurate FEM solution as shown above. Only one conductivity value is varied at a time, and the others remain at the values specified in Table II. The curves in Figure 7 show the errors when the conductivity values of scalp, brain, radial skull, and tangential skull are varied successively. Conductivity variations are quantified with the ratio of the considered value to the middle value used for the model. RDM and MAG have the same definition as in FEM Validation, above, by taking V_{real} as the potential obtained with the middle value of the conductivity and $V_{estimated}$ as the potential obtained with the modified conductivity. Only tangential dipole results are shown, since results for radial and tangential dipoles are very similar.

Figure 7 shows that the influence of the brain and of the radial skull conductivities on the RDM is much more important than that of other conductivities. For brain conductivity, this result is not surprising, since the brain contains the dipoles. This result was obtained by Haueisen et al. [1997] in an isotropic medium. For the radial skull conductivity, the same results were

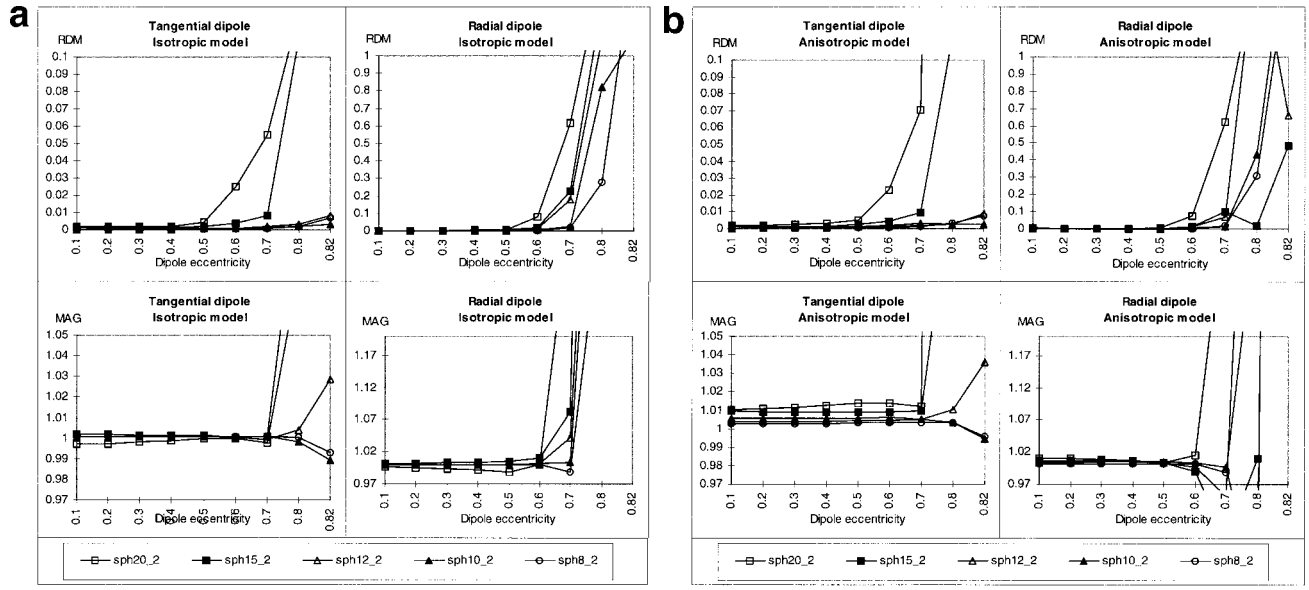

Figure 6.
Errors on the scalp potential distribution calculated with different element size meshes in the case of second-order elements and with V computed in the scalp. Note that the scale used for radial and tangential dipoles are very different. **a:** Isotropic skull. **b:** Anisotropic skull.

obtained by Zhou and van Oosterom [1992]. It should be borne in mind that the absolute value of the errors is very small and not visible on the potential map. It is clear from Figure 7 that the influence of scalp conductivity on the MAG value is very important. Scalp conductivity does not alter the form of the curves but modifies the potential values of these curves. The factor by which the potential increases is inversely proportional to the conductivity, and thus the product (conductivity multiplied by potential) remains constant, implying thereby that scalp conductivity does not cause an error on the dipole localization in the inverse problem.

In conclusion, the two most critical values of conductivity are those of the brain and of the radial skull.

Variations of the conductivity tensor directions

In the spherical case, the conductivity tensor directions are the radial and the tangential directions of the sphere. However, this is not the case with the realistic geometry where the directions of the tensor have to be determined (with some errors, obviously), as explained above. It is then necessary to determine the influence of the tensor directions on the potential. Study was made of the spherical case (where a reference position is given by the radial and the tangential directions of the sphere) with mesh sph10_2 and for a dipole of 0.6 eccentricity. In that case, FEM results show a very good accuracy and the errors will mainly be due to errors in tensor directions. To introduce a direction error, a rotation is applied to the conductivity tensor at each element in the skull. Figure 8 shows errors in the scalp potential when the direction of the tensor is varied. The potential distribution on the scalp is practically as sensitive to the direction of the tensor as it is to the conductivity magnitude. However, in this case a significant change in the location of the maximum is visible. In fact, the same rotation of the tensor was applied to each element, but in a head model where directional errors are randomized, their influence is probably less important. To more specifically estimate the errors introduced by the calculation of the tensor directions in the head model, we calculated a

TABLE III. Time required for computation of a potential distribution on the scalp with an HP C110 workstation

Mesh name	sph20_1	sph15_1	sph12_1	sph10_1	sph8_1	sph20_2	sph15_2	sph12_2	sph10_2	sph8_2
Time (sec)	66	122	207	322	610	80	148	259	412	780

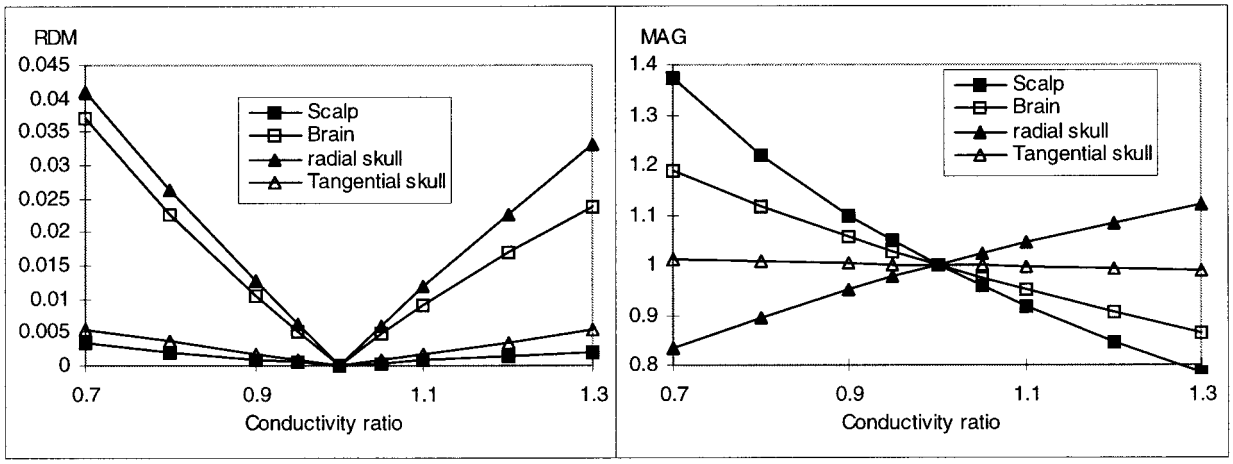

Figure 7.
Error variations on the scalp potential distribution when values of the conductivity vary. The conductivity ratio is the ratio of the considered value to the middle value used for the model.

potential distribution with the spherical model and with a conductivity tensor calculated with exactly the same method as that used for the realistic head model (the tensor directions for each element are calculated using a surface mesh). The results are compared with those obtained by taking the radial and tangential directions of the sphere as the tensor directions. The errors obtained are under 0.2% (RDM $<$ 0.002 and 1 $<$ MAG $<$ 1.005) and produce no visual charge on the potential distribution map.

We thus conclude that the errors introduced in the calculation of the conductivity tensor due to the use of the realistic head model have negligible effects.

Influence of skull anisotropy

Finally, the influence of skull anisotropy was studied in the spherical and the realistic head models. In both cases, the difference in the potential of the scalp is calculated when the skull model is changed from isotropic to anisotropic. The analytical model was chosen for the spherical case, whereas FEM was used for the realistic head model. Figure 9a shows the results in the spherical case. It appears that the influence of skull anisotropy is stronger for radial dipoles than for tangential dipoles. Since the magnification

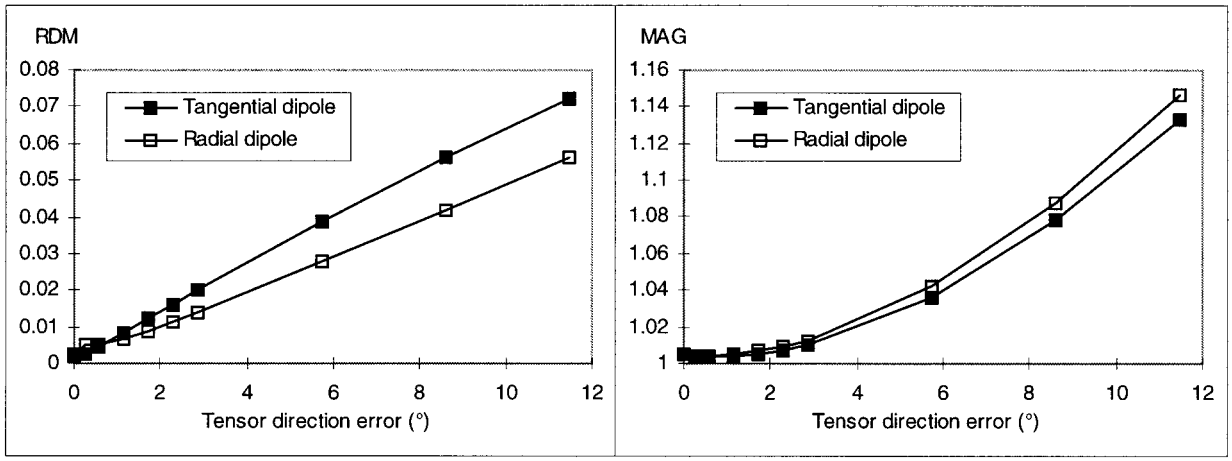

Figure 8.
Error variations on the scalp potential distribution when directions of the conductivity tensor are varied.

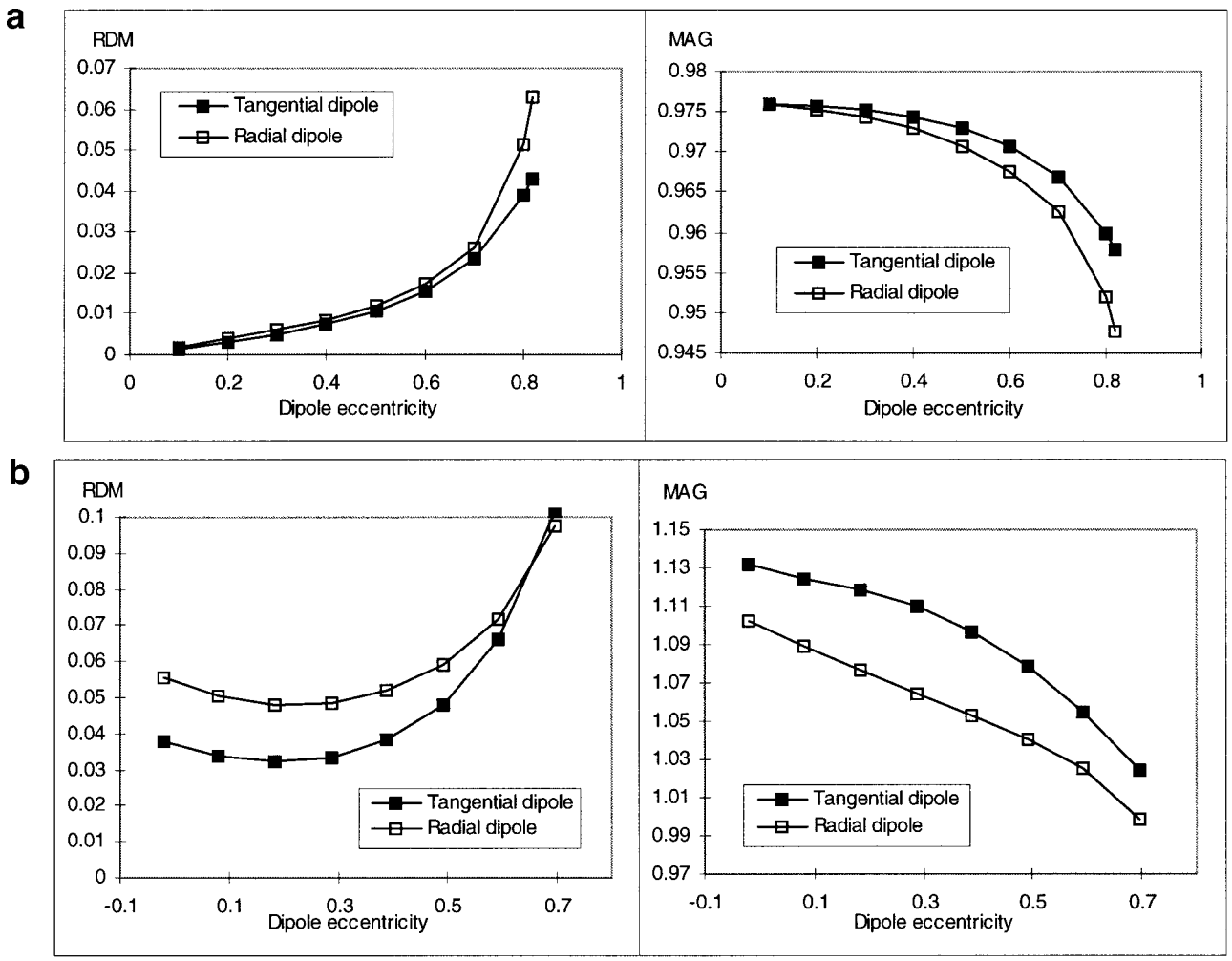

Figure 9.
Errors on the scalp potential distribution due to anisotropic effects. **a:** Spherical case (analytical results). **b:** Realistic head model (FEM results).

factor is less than 1.0, the primary effect of skull anisotropy is to reduce the amplitude of the scalp potential, and this effect is visible even for low-eccentricity dipoles. When the eccentricity increases, anisotropy leads to a greater diffusion of the potential distribution.

Figure 9b shows the errors for the realistic head model. We can point out some differences with the spherical model: the influence of anisotropy with low-eccentricity dipoles is stronger in the realistic head model than in the spherical model. The influence on amplitude is quite different too, since the MAG is now greater than 1.0. Figure 10 shows the potential distribution on the head in the isotropic and the anisotropic cases. It is clear that the potential distribution is still more diffuse in the anisotropic case.

In conclusion, the influence of skull anisotropy is significant for the forward problem, although the errors generally remain lower than 10%. However, the influence of skull anisotropy has to be evaluated for the inverse problem in order to decide whether it has to be taken into account or not.

INFLUENCE OF ANISOTROPY FOR THE INVERSE PROBLEM

The inverse problem has been evaluated in a distributed source model using two different reconstruction methods, one with quadratic regularization and the second with a nonlinear spatial regularization (S-MAP). We here briefly recall the principle of the two regular-

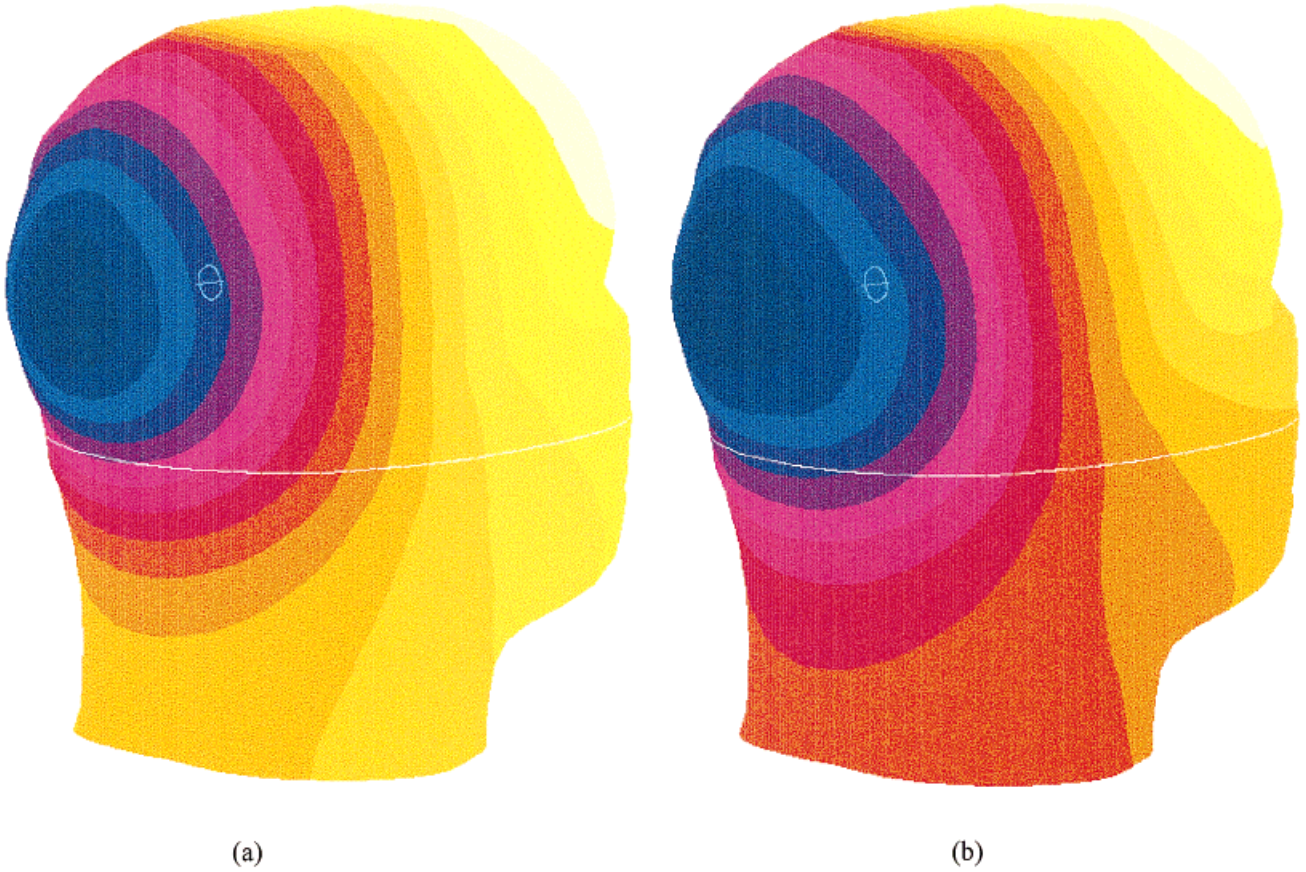

Figure 10.
Potential distribution of **(a)** isotropic model and **(b)** anisotropic model, both with computation of V in the scalp.

ization methods applied to the EEG/MEG inverse problem.

The inverse problem of EEG source estimation is ill-posed because of two main reasons.

First, the solution is not unique: very different source configurations can give a highly satisfactory fit to data. Second, the solution is not stable with regard to small changes on data. In other words, the solution does not continuously depend on data values.

For a distributed source model, these two statements are due to the bad conditioning of the linear operator (the gain matrix) that binds source amplitudes to the sensor array. Basically, a regularization process tends to reduce the oscillatory behavior of the solutions of linear equation systems with bad conditioned operators and noisy data sets. A regularized solution of the following linear system

$$\boldsymbol{M} = \boldsymbol{GJ} + \boldsymbol{b},$$

may be expressed as follows:

$$\hat{\boldsymbol{J}} = \arg\min_{J}\{\|\boldsymbol{M} - \boldsymbol{GJ}\|^2 + \lambda\|L(\boldsymbol{J})\|^2\},$$

Here $\boldsymbol{M}$ stands for the data set, $\boldsymbol{G}$ for the gain matrix, $\boldsymbol{J}$ is the dipole magnitude vector, and $\boldsymbol{b}$ is a model of additive Gaussian white noise.

$L(.)$ is the regularization operator that may be linear or nonlinear and describes the type of priors one has on the shape of the solution. (λ expresses the relative importance of the a priori with regard to data attachment.

Quadratic regularization is one of the most popular techniques [Tikhonov and Arsenin, 1977]. Though this technique introduces weak priors with operators (weighted or not) such as identities, gradients, or laplacians of dipole amplitudes, and is easy to implement, it tends to smear and to overestimate the spatial extension of the active sources. Moreover, the

so-called minimum norm techniques such as the constrained inverses of matrices for least-square solutions of linear systems [Rao and Mitra, 1973] offer the same type of oversmoothed dipole intensity patterns [Pascual-Marqui et al., 1994] as those produced by the quadratic regularization methods.

When the $L(.)$ operator is nonlinear, it is possible to introduce more sophisticated priors on the source distribution such as the preservation of anatomo-functional discontinuities that can provide relevant information on the cognitive process. The original S-MAP method is extensively described in Baillet and Garnero [1997] and may be briefly exposed as follows.

$L(.)$ is now expressed as the sum of locally defined cost functions associated with each intensity gradient in the dipole image. These cost functions are locally scaled so that in some areas, high-intensity jumps are more likely to be created than in others. For instance, it is possible to allow intensity gradients between two walls of a sulcus. Finally, the general shape of S-MAP solutions is made of areas with slowly varying intensity and which may be separated by strong discontinuities.

These two reconstruction methods are used in three different situations. Twelve a priori active areas have been isolated in a three-shell head model from selective attention auditory experimental data. The corresponding cortex patchwork is shown in Figure 11.

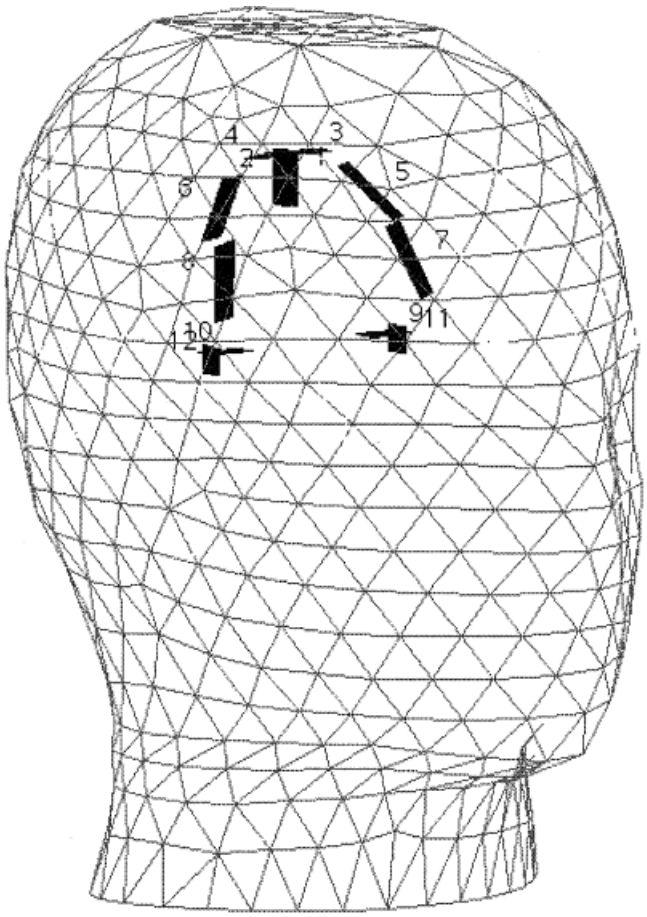

Figure 11.
Cortex patches representing a priori active areas of the brain, isolated owing to anatomical MRI and PET imaging in an auditory experiment. These patches are located in temporal auditory and motor cortex areas.

Forty-eight dipoles (four per patch) are spread perpendicularly over these surfaces. For simplicity, the same number of dipoles is put on each patch, and only configurations where all dipoles of a patch are in the same state, illuminated or not, are chosen. The EEG recording is simulated on a 70-electrode set with the anisotropic model using the dipole amplitudes shown in Figure 12.

The three different activity patterns have been simulated in order to test different situations. In the first case (Fig. 12a), the efficiency of the algorithm to distinguish between two close and simultaneous activations with different orientations is tested. This corresponds, for instance, to a simultaneous response in the internal and upper part of the motor area, or in two perpendicular walls of the calcarine scissure. In the second case (Fig. 12b), the active areas are well-separated but they have the same direction. The third case (Fig. 12c) is the most complex and corresponds to a distributed activity over four active areas with different directions.

Preliminary reconstructions, carried out with the suitable anisotropic models, show that electrical activity can be accurately recovered in all cases with either of the two regularization methods; this is so since no additive noise is introduced and since the problem is well-determined (the number of dipoles is smaller than the number of data). Reconstructions presented in this paper are made with isotropic models, whereas EEG recording is still calculated with anisotropic models. Thus, the errors for having neglected skull anisotropy can be evaluated.

Spherical model

The influence of anisotropy on the inverse problem is first estimated in a spherical model. Since the forward problem is analytically calculated in this case, possible errors in the inverse problem will be due to anisotropy effects only. Resulting dipole amplitudes are shown in Figure 13a for the quadratic regularization method and in Figure 13b for S-MAP, each case

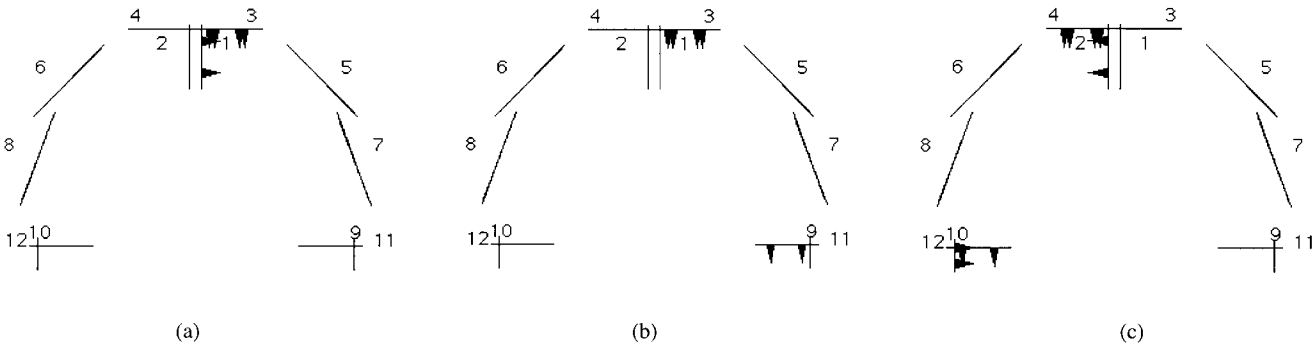

Figure 12.

Three different activity patterns of dipole amplitudes used to calculate the simulated EEG data. Illuminated dipoles are represented as solid triangles. These patterns are the activity to be recovered in the inverse problem. **a:** Two close patches with orthogonal directions are illuminated. **b:** Two well-separated patches with the same direction are illuminated. **c:** More complex pattern with four patches illuminated.

respectively corresponding to the cases of Figure 12 where the real dipole amplitudes used to simulate the EEG recording are shown. With quadratic regularization (Fig. 13a), reconstructed electrical activity is spread all around the cortex, and the amplitudes of the dipoles in the active areas are strongly attenuated. The first case is the only one where an acceptable solution is found, although the electrical activity is weak, even in this case. The bias introduced by the model error (isotropic conductivities) on the inverse problem appears to be strong and it is necessary to use a more sophisticated regularization method such as the nonlinear one. Figure 13b shows the results obtained with S-MAP. The first two cases are well-reconstructed, though the dipole amplitudes were slightly underestimated (0.8–0.9 instead of 1). This was expected, because the potential maxima are smaller in the anisotropic case (see Fig. 9). Moreover, regularization tends to minimize the dipole amplitudes, and the two effects add together. In the last case of Figure 13b, electrical activity is found on patches one and two, but the sum of the two activities approximately corresponds to the activity assigned to patch two. Parasite activity is also found on patch 5. Although the results are better than those obtained with quadratic regularization, the spread of electrical activity may not be negligible in this case, with what could be called a loss in the spatial resolution of EEG imaging due to the use of an approximate head model.

FEM realistic head model

Resulting dipole amplitudes are shown in Figure 14a,b for the quadratic regularization and S-MAP, respectively. As with the spherical model, quadratic regularization cannot correctly recover the electrical activity. The result is even worse in the first pattern of Figure 14a (compared to the first pattern of Fig. 13a), probably because of a more diffuse distribution caused by anisotropy in the realistic model than in the spherical one. Figure 14b presents the S-MAP results and shows that the electrical activity is perfectly recovered for the second pattern only. In the first pattern, the activity found on patch 2 corresponds to the activity assigned to patch 1. When patch 1, or patch 2, or both are illuminated, our algorithm always chooses patch 2. This problem was not observed with the spherical model and may be the solution given to the more extended diffusion due to anisotropy with the nonsymmetric geometry of the head. In the last pattern of Figure 14b, patch 10 is overestimated (1.3 for 1), and the activity on patch 4 is spread to patch 3. Activity on patch 2 is strongly underestimated (0.5 for 1). As in the spherical model, anisotropy has nonnegligible influence on the inverse problem with the last pattern of Figure 14b.

In conclusion, the quadratic regularization method is not sufficient for recover electrical activity, when bias of skull anisotropy is introduced. S-MAP provides accurate results in the case of sparse spot activity, but complex activity distribution is recovered with strong parasite activity on adjacent patches, although results are better than those obtained with quadratic regularization. This parasite activity may have disastrous consequences and may be considered nonacceptable in many neuropsychological imaging experiments.

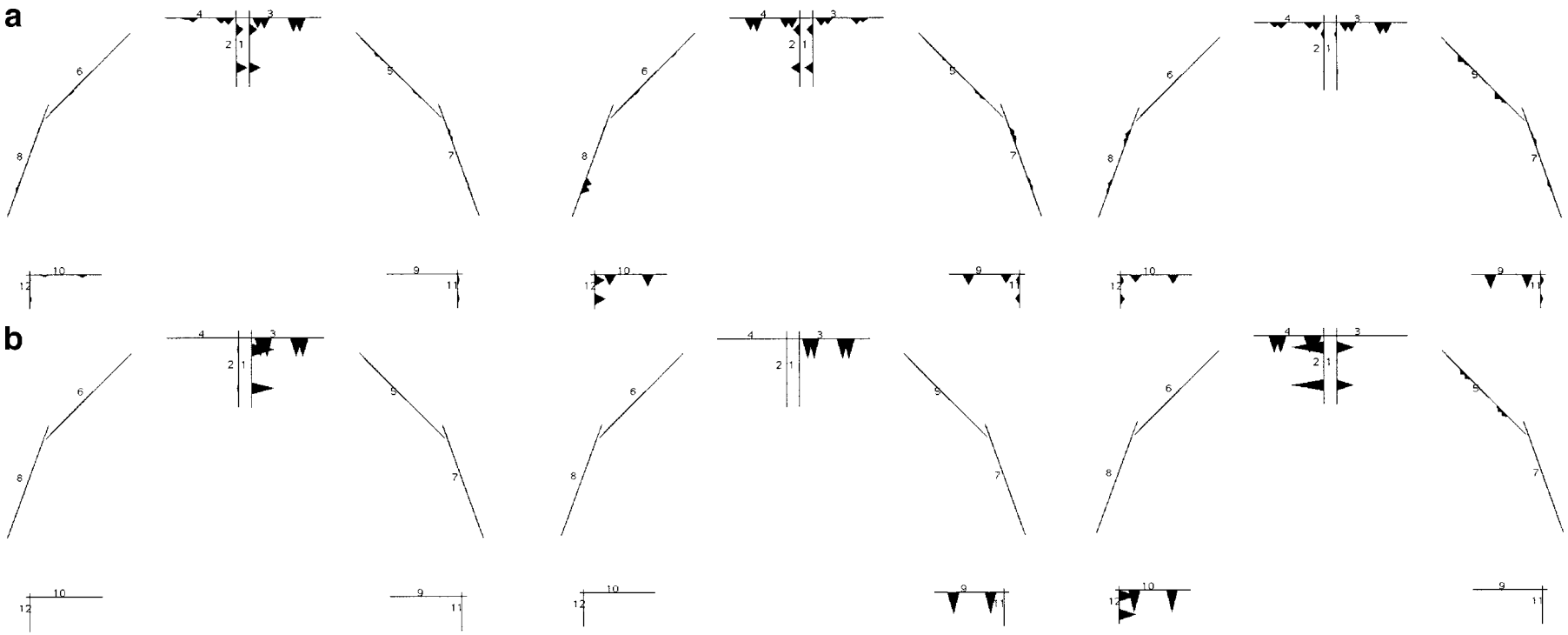

Figure 13.

Reconstructed dipole amplitudes in the spherical case. **a:** With the minimum norm regularization method. **b:** With the nonlinear regularization method. The three patterns in a and in b correspond respectively, to the three cases in Figure 12.

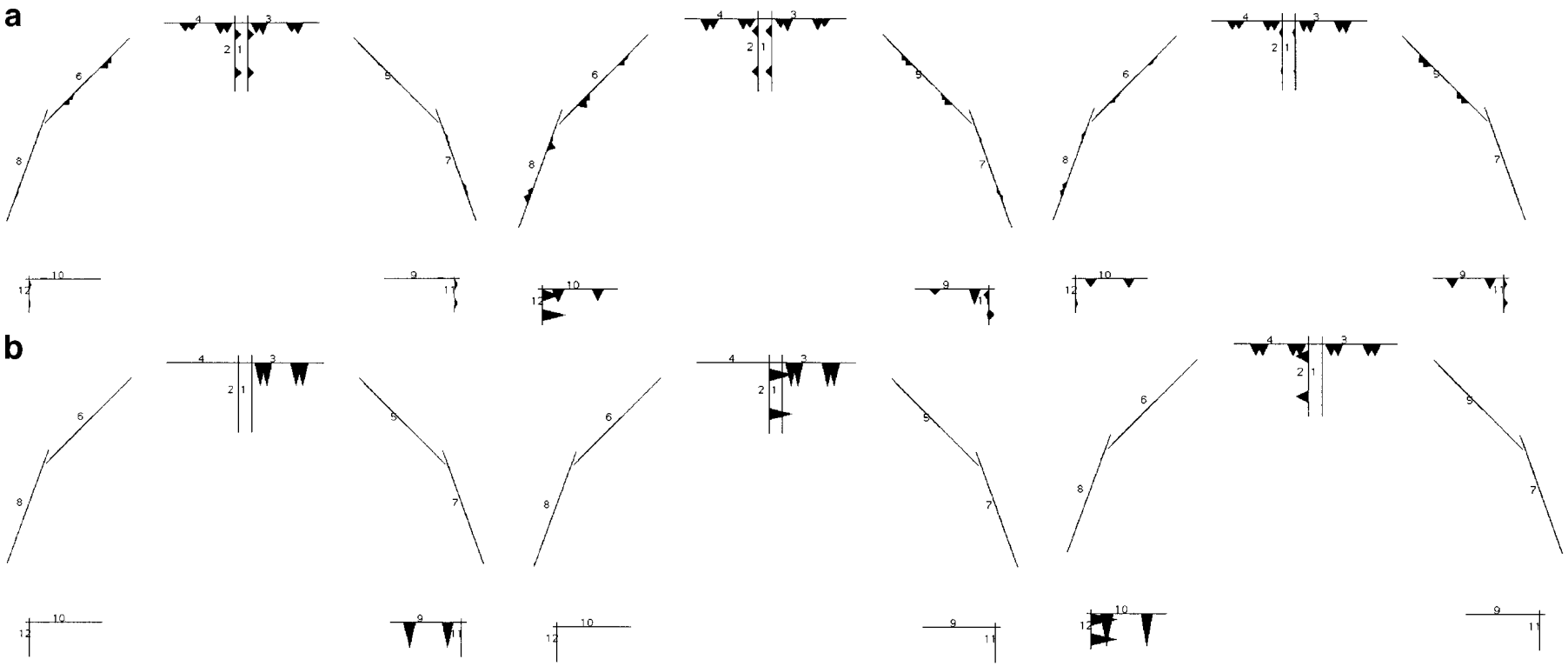

Figure 14.
Reconstructed dipole amplitudes in the realistic head case. **a:** With the minimum norm regularization method. **b:** With the nonlinear regularization method. The three patterns in a and in b correspond, respectively, to the three cases in Figure 12.

DISCUSSION

First of all, the influence of skull anisotropy on scalp potential distribution in spherical and realistic head models has been studied. For this purpose, a finite element method has been implemented, and validated in a spherical head model by comparing the results with the analytical ones. The optimum parameters of the method have been estimated, and we have shown that good accuracy can be obtained for radial and tangential dipoles of eccentricity lower than 0.7, which approximately corresponds to dipoles lying in the middle of the cortex.

The influence of skull anisotropy has been evaluated, when tangential conductivity is 10 times higher than radial conductivity. The potential distribution due to a single dipole is more diffuse with an anisotropic skull. The influence of anisotropy is stronger for more eccentric dipoles, since they are located closer to the skull (and especially radial sources). In the spherical case, anisotropy tends to attenuate the amplitude of the potential, whereas it overestimates it in the case of the realistic head model. But in general, the difference between isotropic and anisotropic cases is not dramatic from this quantitative point of view (the RDM does not exceed 10% in the worst case), and is of the same order as that due to other modelization errors, e.g., the presence of skull holes.

Nevertheless, the gain matrix derived from the isotropic conductivity model (such as the one computed with the boundary element method) introduces bias in the inverse problem solutions. This bias has been evaluated in a distributed source model for which source reconstruction means solving an ill-posed linear equation system. Since the gain matrix does not perfectly translate the real model, the inversion needs to be regularized in order to get stable solutions, even if data are noiseless and the linear system completely determined.

Simulated source distributions have been reconstructed with modelling errors: data were generated with an anisotropic model, while sources were computed with the associated isotropic model gain matrix. The solutions presented here were obtained using two regularization methods: a quadratic regularization technique which acts as a minimum norm method, and a nonlinear method we have developed in a previous work [Baillet and Garnero, 1987].

The solutions found with the quadratic regularization method are spread over the cortical surface, and the estimated dipole amplitudes are attenuated. This effect is essentially due to the need for strong regularization induced by a wrong gain matrix and to the constraints used for the regularization, i.e., the minimization of the dipole vector norm. The main effect is to smooth the solutions, and even two distinct activities of different orientations or separate locations cannot be distinguished.

Nonlinear regularization allows one to introduce more a priori information. Not only smoothed intensity distributions, but also a larger variety of dipole distributions, can thus be recovered. The hypothesis of source distribution assumed in our method is that the distribution of activity is composed of piecewise homogeneous patterns, which is a physiologically correct assumption.

S-MAP can accurately recover sparse spots with different or identical orientations, even with an isotropic model. However, the dipole amplitudes cannot be exactly estimated since anisotropic conductivity tends to change the magnitude of the surface potential. Moreover, as an anisotropic model produces a greater diffusion of the scalp potential than the isotropic model assumed for the reconstruction, the estimated activity is spread on larger areas so that activities in adjacent cortical regions cannot be separated. If skull anisotropy is not taken into account in the head model, the inverse method will thus fail to produce a precise representation of different functional areas along a cortical fold, or to describe the diverse areas simultaneously involved in a complex cognitive task, or even to accurately localize a response between two adjacent sulci or gyri. Even with a nonlinear regularization technique and strong a priori information, complex activity distributions made of different spots with similar contributions to the data cannot be accurately estimated if anisotropy is not taken into account.

More generally, the direct problem is far from being accurate and gives a very simplified picture of the head, which is in reality a highly complex structure. Many improvements have to be introduced in the realistic head model so that it can take into account local conductivity inhomogeneities such as the presence of holes in the skull or the high conductivity of the ventricles. Nevertheless, due to the uncertainties in conductivity values, specific regularization methods should be developed at the same time. It is thus necessary to simultaneously develop, for the EEG inverse problem, regularization methods less sensitive to modelization errors with distinct origins and effects on the data. This will be possible only if a priori assumptions can be made on the activity pattern. Furthermore, following the results of this study, it is now possible to explicitly include in the inverse priors a model of data deformation produced by simplified

models in a real human head. This will be done specifically in the context of the Bayesian formulation used by S-MAP.

We are currently investigating a similar study for MEG direct and inverse problems.

ACKNOWLEDGMENTS

The authors gratefully acknowledge S. Mallick, S. Margules, and B. Renault for attentive reading of the manuscript.

REFERENCES

Awada KA, Jackson DR, Williams JW, Wilton JR, Baumann SB, Papanicolaou AC (1997): Computational aspects of finite element modeling in EEG source localization. IEEE Trans Biomed Eng 44:736–751.

Baillet S, Garnero L (1997): A Bayesian approach to introducing anatomo-functional priors in the EEG/MEG inverse problem. IEEE Trans Biomed Eng 44:374–385.

Bertrand O, Thevenet M, Perrin F (1991): 3D finite element method in brain electrical activity studies. In: Nenonen J, Rajala HM, Katila T (eds): Biomagnetic Localization and 3D Modelling, Report of the Department of Technical Physics, Helsinski University, pp 154–171.

Buchner H, Knoll G, Fuchs M, Rienaäcker A, Beckmann R, Wagner M, Silny J, Jörg P (1997): Inverse localization localization of electric dipole current sources in finite element models of the human head. Electroencephalogr Clin Neurophysiol 102:267–278.

Dale AM, Sereno MI (1993): Improved localization of cortical activity by combining EEG and MEG with MRI cortical surface reconstruction: A linear approach. J Cogn Neurosci 5:162–176.

De Munck JC (1988): The potential distribution in a layered anisotropic spheroidal volume conductor. J Appl Physiol 64:464–470.

Gorodnitsky IF, George JS, Rao BD, (1995): Neuromagnetic imaging with FOCUSS: A recursive weighted minimu-norm algorithm. Electroencephalogr Clin Neurophysiol 79:211–226.

Hämäläinen MS, Ilmnoniemi RJ (1994): Interpreting magnetic fields of the brain: Minimum norm estimated. Med Biol Eng Comp 32:35–42.

Hämäläinen MS, Sarvas J (1989): Realistic conductivity geometry model of the human head for interpretation of neuromagnetic data. IEEE Trans Biomed Eng 86:165–171.

Haueisen J, Ramon C, Czapski P, Eiselt M (1995): On the influence of volume currents and extended sources on neuromagnetic fields: A simulation study. Ann Biomed Eng 25:728–739.

Haueisen J, Ramon C, Eiselt M, Brauer H, Nowak H (1997): Influence of tissues resistivities on neuromagnetic fields and electric potentials studied with a finite element model of the head. IEEE Trans Biomed Eng 44:727–735.

Meijs JWH, Weier OW, Peters MJ, Oosterom AV (1989): On the numerical accuracy of the boundary element method. IEEE Trans Biomed Eng 36:1038–1049.

Miller CE, Henriquez CS (1990): Finite element analysis of bioelectric phenomena. Crit Rev Biomed Eng 18:207–233.

Pascual-Marqui RD, Michel CM, Lehmann D (1994): Low resolution electromagnetic tomography: A new method for localizing electrical activity of the brain. Int J Psychophysiol 18:49–65.

Peters MJ, de Munck JC (1990): The influence of model parameters on the inverse solution based on MEGs and EECs. Acta Otolaryngol [Suppl] (Stockh) 491:61–69.

Rao CR, Mitra SK (1973): Theory and application of constrained inverses of matrices. SIAM J Appl Math 24:476–488.

Sarvas J (1987): Basic mathematical and electromagnetic concepts of the biomagnetic inverse problem. Phys Med Biol 32:11–22.

Sherg M, Buchner H (1993): Somatosensory evoked potentials and magnetic fields: Separation of multiple source activity. Physiol Measurements [Suppl] 14:35–39.

Simkin J, Trowbridge CW (1979): On the use of the total scalar potential in the numerical solution of fields problems in electromagnetics. Int J Num Methods Eng 14:423–440.

Thevenet M (1992): Modélisation de l'activité électrique cérébrale par la méthode des éléments finis. Thèse, no. d'ordre 92 ISAL 0036.

Tikhonov A, Arsenin V (1977): Solutions of Ill-Posed Problems. Washington, DC: Winston.

Wang JZ, Williamson SJ, Kaufman L (1992): Magnetic source images determined by a lead-field analysis: The unique minimum-norm least-squares estimation. IEEE Trans Biomed Eng 39:665–675.

Wikswo JR, Gevims A, Williamson SJ (1993): The future of EEG and MEG, Electroenceph Clin Neurophysiol 87:1–9.

Yan Y, Nunez PL, Hart RT (1991): Finite element model of the human head: Scalp potentials due to dipole sources. Med Biol Eng Comp, 1991 29:475–481.

Zhou H, van Oosterom A (1992): Computation of the potential distribution in a four-layer anisotropic concentric spherical volume conductor. IEEE Trans Biomed Eng 39:154–158.

Zienkiewicz OC (1977): The Finite Element Method in Engineering Science. McGraw-Hill, New York.

Zubal IG, Harrell CR, Smith EO, Rattner Z, Gindi GR, Hoffer PB (1994): Computerized three-dimensional segmented human anatomy. Med Phys 21:299–302.

APPENDIX

Forward problem equations

We consider the head to be composed of different media k which can be isotropic or anisotropic, each medium being characterized by a conductivity tensor $[\sigma_k]$. The surface between the media k and k + 1 is noted S_k. The problem of a current dipole in a conductor is formulated as follows:

$$\boldsymbol{J} = \boldsymbol{J_i} + \boldsymbol{J_c} = \boldsymbol{J_i} + [\sigma]\boldsymbol{E} = \boldsymbol{J_i} - [\sigma]\boldsymbol{gradV}, \qquad (1)$$

where $\boldsymbol{J}$ is the total current density, $\boldsymbol{J_i}$ the current density imposed by the dipole source (which is non-zero only at the dipole location), $\boldsymbol{J_c}$ the ohmic current density, $[\sigma]$ the conductivity tensor at each point of the volume, and V the scalar potential derived from the electric field $\boldsymbol{E}$ ($\boldsymbol{rotE} = \boldsymbol{0}$). In the quasistatic approximation which is valid in the EEG case, the current $\boldsymbol{J}$ is determined by the equation:

$$div\boldsymbol{J} = 0 \qquad (2)$$

with the following boundary conditions:

$$V_k|_{S_k} = V_{k+1}|_{S_k}$$

$$[\sigma_k]\boldsymbol{grad}V_k|_{S_k} \cdot \boldsymbol{n_k} = [\sigma_{k+1}]\boldsymbol{grad}V_{k+1}|_{S_k} \cdot \boldsymbol{n_k},$$

where $\boldsymbol{n_k}$ is the vector normal to the surface S_k. If we suppose that the dipole is located in a homogeneous isotropic medium (which is a rather good assumption since the dipoles are in the cortex), Equation (2) in the dipole region is written as:

$$div(\sigma_1 \boldsymbol{grad} V) = div\boldsymbol{J_i}, \tag{3a}$$

(σ_1 being the scalar conductivity of this region). In other regions (which do not contain dipoles), Equation (2) becomes:

$$div([\sigma]\boldsymbol{grad} V) = 0. \tag{3b}$$

A singularity appears at the dipole position which may cause numerical problems. A classical way to avoid this singularity is to split the potential V in two parts as follows:

$$V = U + V_S \tag{4}$$

where V_s, called the ''singular solution,'' is the potential due to the dipole in an infinite homogeneous medium that has the same conductivity as that of the medium containing the dipoles; U, called the ''regular solution'' or ''reduced potential,'' remains finite at each point. Since V_s is a solution of Equation (5a), the equations to be solved become:

$$div(\sigma_1 \boldsymbol{grad} U) = 0 \quad \text{in medium 1} \tag{5a}$$

$$div([\sigma_n]\boldsymbol{grad}U) = -div([\sigma_n]\boldsymbol{grad}V_S) \quad \text{in media } n \neq 1. \tag{5b}$$

The singularity in medium 1 disappears for U.

In some media that contain no dipole (n / 1), we can directly compute V, called ''total potential,'' since there is no singularity. The equation to be computed in these media is then:

$$div([\sigma_n]\boldsymbol{grad} V) = 0 \quad \text{in media } n \neq 1 \tag{5c}$$

The potential V_s induced by a dipole of moment $\boldsymbol{Q}$, at a point $\boldsymbol{r}$, different from the dipole position $\boldsymbol{r_0}$, is given by the analytical expression [Sarvas, 1987]:

$$V_S(\boldsymbol{r}) = \frac{1}{4\pi\sigma_1}\boldsymbol{Q} \cdot \frac{\boldsymbol{r} - \boldsymbol{r_0}}{|\boldsymbol{r} - \boldsymbol{r_0}|^3}.$$

Finite element formulation

Here is presented a brief overview of the method. The problem is first considered in a well-suited form for FEM. The integral form of the continuous problem formulated in Equation (2) on a volume conductor Ψ can be written as [Zienkiewicz, 1977; Miller and Henriquez, 1990]:

$$\forall \Psi \in W, \quad \int_\Omega \boldsymbol{J} \cdot \boldsymbol{grad}\Psi \, d\Omega = 0, \tag{6}$$

where W is a set of admissible functions Ψ defined on the volume Ω. We now consider the case of media where U is computed. By using Equation (4), Equation (6) becomes:

$$\int_\Omega \boldsymbol{grad}\Psi \cdot [\sigma]\boldsymbol{grad}U \, d\Omega = -\int_\Omega \boldsymbol{grad}\Psi \cdot [\sigma]\boldsymbol{grad}V_S \, d\Omega, \quad \forall \Psi \in W, \tag{7}$$

The right-hand side of Equation (7) is a volume integral valid both in isotropic and in anisotropic media. For isotropic homogeneous medium, it can easily be transformed into a surface integral using Green's theorem:

$$\int_\Omega \boldsymbol{grad}\Psi \cdot [\sigma]\boldsymbol{grad}U \, d\Omega = -\int_{\Gamma_i} \Psi\sigma\boldsymbol{grad}V_S \cdot \boldsymbol{n_{i_{iso}}} \boldsymbol{d}\Gamma_{i_{iso}}$$

where $\Gamma_{i_{iso}}$ is the surface of an isotropic part of Ω with normal vector (pointing out of $\Gamma_{i_{iso}}$). For a volume Ω containing both isotropic and anisotropic media, two terms appear:

$$\int_\Omega \boldsymbol{grad}\Psi \cdot [\sigma]\boldsymbol{grad}U \, d\Omega = -\int_{\cup\Omega_{i_{aniso}}} \boldsymbol{grad}\Psi \cdot [\sigma]\boldsymbol{grad}V_S \, d\Omega - \sum_{i_{iso}} \int_{\Gamma_{i_{iso}}} \Psi\sigma\boldsymbol{grad}V_S \cdot \boldsymbol{n}_{i_{iso}} \, d\Gamma_{i_{iso}} \tag{8}$$

where $\cup\Omega_{\text{ianiso}}$ is the fraction of volume Ω that has anisotropic or inhomogeneous conductivities.

In FEM, the continuous problem is approximated by a discretized problem in a subset of W. In practice, the domain Ω is split into elements and nodes, and a basis function w_i of is associated with each node i. These functions can either be linear functions defined on first-order elements or parabolic functions defined on second-order elements. The functions Ψ are replaced by the basis functions w_i and the solution U is approximated by where $U_\alpha = \Sigma_{i=1}^{N} u_i w_i$, N being the number of nodes, and u_i the value of U at the node i [Zienkiewicz, 1977]. Equation (8) becomes a linear system of N equations with N unknowns:

$$[R][U] = [S] \tag{9}$$

where $[U]$ is a vector with components u_i, $[R]$ a $N \times N$ matrix, and $[S]$ a $1 \times N$ matrix. These matrices are calculated as follows:

$$R_{ij} = \int_\Omega \mathbf{grad} w_i \cdot [\sigma] \mathbf{grad} w_j \, d\Omega,$$

$$S_j = -\int_{\cup \Omega_{i_{aniso}}} \mathbf{grad} w_j \cdot [\sigma] \mathbf{grad} V_S \, d\Omega - \sum_{i_{iso}} \int_{\Gamma_{i_{iso}}} w_j \sigma \mathbf{grad} V_S \cdot \mathbf{n_{i_{iso}}} \, d\Gamma_{i_{iso}}.$$

Remark

For media where the total potential V is computed, similar transformations are made and an equivalent linear system is solved:

$$[R][V] = 0,$$

where $[R]$ is the same matrix as in Equation (9).

These methods are similar to the ''reduced and total scalar potential methods'' used to compute the magnetic scalar potential in magnetostatic problems [Simkin and Trowbridge, 1979].